

Title	Distributed hierarchical droop control of boost converters in DC microgrids
Authors	O'Keefe, Daniel;Riverso, Stefano;Albiol-Tendillo, Laura;Lightbody, Gordon
Publication date	2017-07-20
Original Citation	O'Keefe, D., Riverso, S., Albiol-Tendillo, L. and Lightbody, G. (2017) 'Distributed hierarchical droop control of boost converters in DC microgrids', 28th Irish Signals and Systems Conference (ISSC), Killarney, Ireland, 20-21 June 2017, 1-6. doi:10.1109/ISSC.2017.7983615
Type of publication	Conference item
Link to publisher's version	10.1109/ISSC.2017.7983615
Rights	© 2017 IEEE. Personal use of this material is permitted. Permission from IEEE must be obtained for all other uses, in any current or future media, including reprinting/republishing this material for advertising or promotional purposes, creating new collective works, for resale or redistribution to servers or lists, or reuse of any copyrighted component of this work in other works.
Download date	2023-05-05 20:56:11
Item downloaded from	http://hdl.handle.net/10468/5424



UCC

University College Cork, Ireland
Coláiste na hOllscoile Corcaigh

Distributed Hierarchical Droop Control of Boost Converters in DC Microgrids

Daniel O’Keeffe[†], Stefano Rivero[‡], Laura Albiol-Tendillo[‡], Gordon Lightbody^{†§}

[†]Control & Intelligent Systems Group, School of Engineering, University College of Cork, Ireland

[‡]United Technologies Centre Ireland Ltd, 4th Floor Penrose Business Centre, Cork, Ireland

[§]MaREI-SFI Research Centre, University College Cork, Cork City, Ireland

Email: danielokeeffe@umail.ucc.ie

Abstract—Voltage stability and accurate current-sharing are primary features of an efficiently operating power distribution network, such as a dc islanded-microgrid. This paper presents the development of a distributed hierarchical droop control architecture for dc-dc boost converters within a dc islanded-microgrid. Decentralised controllers are conventionally designed for local voltage and current control without accounting for coupling to other converters. However, due to the non-minimum phase action of boost converters, global knowledge of coupling is required to inform stable local controller tuning over a range of load disturbances. Consensus-based distributed secondary controllers, utilising low-bandwidth communications, are designed to coordinate voltage levels and improve current-sharing accuracy. The control architecture is tested in response to communication faults, non-linear loads, and plug-and-play operations.

Index Terms—low-voltage dc microgrids, distributed control; voltage stability, current-sharing; consensus algorithms.

I. INTRODUCTION

THE proliferation of deregulated markets, distributed generation units (DGU), active consumer participation, advances in distributed storage units (DSU) and power electronics has led to the development of microgrids (mGs) as a way to autonomously integrate, manage and efficiently distribute power [1]. Extensive research conducted on ac mGs has naturally progressed [2], [3], as ac power is deeply embedded in society. However, inherent issues such as harmonics, power imbalances, reactive power control and synchronisation are avoided when operating with dc. Furthermore, most renewable DGUs (rectified-wind, solar and fuel cell power), DSUs (batteries, flywheels, super-capacitors) and loads (electric vehicles, electronic loads, variable speed drives), intrinsically operate with dc. As a result, dc power distribution can achieve greater reliability, resiliency, and power quality compared to ac.

DC mGs vary in size, from small-scale low voltage dc (LVDC) networks such as mobile phones, rooms/buildings/residential households to large-scale systems such as data centres, avionics and commercial & industrial (C&I) buildings. Recently, dc ImGs have been deployed in LVDC networks such as telecom towers, occupied interior spaces, data centres and traction systems [4]–[7]. Currently, research initiatives are focusing on the roll-out of residential and C&I building mGs [8]. Furthermore, dc mGs are being applied in HVDC networks, on-board maritime vessels [9] and multi-terminal dc links [10].

From a control perspective, the integration of stochastic renewable resources and lack of inertia in mGs challenges

the voltage stability of power converters that interface DGUs, DSUs and loads [11]. Furthermore, accurate current-sharing between these elements is required to achieve efficient operation. A hierarchical control structure has successfully been implemented in LV small-scale ac and dc mGs [2], [12]. The control hierarchy of mGs consists of inner, primary and secondary control layers implemented with classical single-input-single-output (SISO) controllers. The inner control layer consists of fast local voltage and current controllers for regulating local power levels. Primary control complements this layer by adding an additional feedback loop to handle current-sharing between DGUs. These control layers are decentralised, improving reliability without peer-to-peer communication. Distributed secondary controllers coordinate voltage levels and improve current-sharing accuracy using low-bandwidth communications.

Existing control issues concerning the deployment of large-scale mGs include scalability, reconfigurability, cooperation and fault-tolerance [11]–[13]. Scalable designs improve the modularity of mGs, meaning that the design of local controllers does not depend on global knowledge or complexity of the mG. Reconfiguration of devices and communication channels is a critical feature in large-scale systems in order to achieve resiliency, dynamic performance and fault-tolerance.

The objective of this paper is to extend the existing control architecture to dc-dc boost converters, and to evaluate voltage and current-sharing performance within the context of large-scale mG issues. Initially, fully decentralised primary controllers are designed. Relative gain array (RGA) analysis is performed to determine the level of interaction between decentralised controlled DGUs. Global knowledge of line coupling is required in order to account for the line dependent non-minimum phase action, which severely reduces the closed-loop bandwidth and necessitates controller detuning. The impact of communication faults highlight the importance of fault-tolerance. Voltage restoration and current-sharing accuracy are tested with the addition of a non-linear dc motor load. Finally, the plug-and-play (PnP) capabilities of the control scheme are examined by adding/removing DGUs and loads to the dc mG.

II. DC MICROGRID CONFIGURATION

DC mGs are generally coupled to the stiff utility grid through power converter units, which effectively islands the dc mG. A fundamental feature of any islanded-mG (ImG) is

the ability to convert power between different DGUs, DSUs and loads automatically and efficiently. Within a dc ImG, this is performed using different dc-dc boost and buck converter topologies. Fig. 1 presents the general configuration of a radial dc ImG that can exchange power with the utility grid.

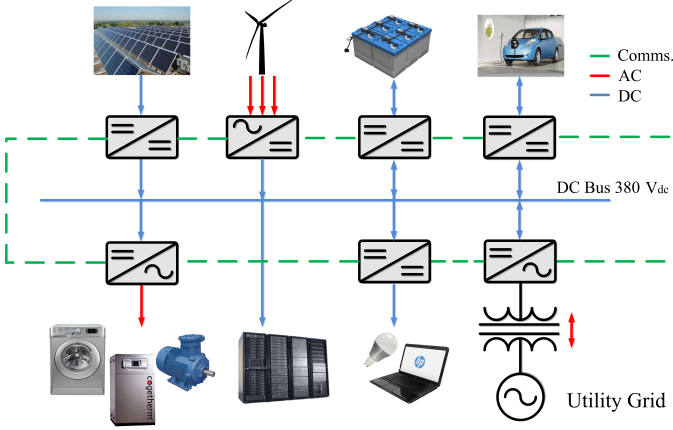


Fig. 1. Radial configuration of a LVDC microgrid. Adapted from [14].

Ultimately, key to enabling intelligent and autonomous operation of a dc ImG is the control and coordination of the power converters interfacing equipment. This work considers dc-dc boost converters.

III. DC-DC BOOST CONVERTER MODEL & CONTROL

DC ImG research predominantly consists of dc-dc buck converters [11]–[15]. Recently, dc-dc boost converter control within a dc ImG has been implemented [16]. However, [16] neglects the interactions between coupled DGUs.

The ideal circuit topology of a boost converter is shown in Fig.2. The output voltage, $v_{dc_i} = \frac{v_{in_i}}{1-d_i}$, can be controlled by adjustment of the duty cycle d_i using pulsewidth-modulation (PWM).

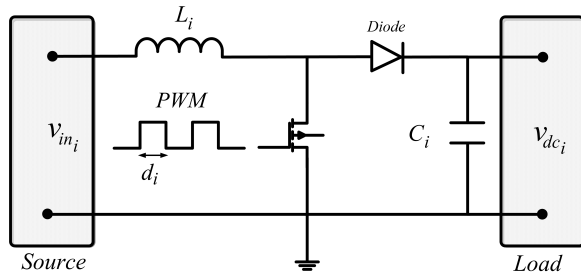


Fig. 2. Ideal unidirectional dc-dc boost converter circuit

Operating in continuous conduction mode (CCM), the boost converter can be represented by a small-signal model [17]. The small-signal duty cycle, \tilde{d}_i (where $d_i = D_i + \tilde{d}_i$) to output voltage transfer function (TF) is given as:

$$\frac{\tilde{v}_{dc_i}(s)}{\tilde{d}_i(s)} = \frac{-V_{in_i}(s - \frac{(1-D_i)R_L}{L_i})}{L_i C_i (s^2 + \frac{1}{R_L C_i} s + \frac{(1-D_i)^2}{L_i C_i})}. \quad (1)$$

This model represents the load as a linear resistive load R_L .

The non-minimum phase action attributed to boost converters is associated with the indirect energy transfer from the

inductor to capacitor during switching. This effect, modelled in (1) as a right-half-plane (RHP) zero of frequency $\omega_{rhp_i} = \frac{(1-D_i)R_L}{L_i}$, limits the achievable closed-loop bandwidth.

Type II and III compensators are commonly used in power converter control where phase injection is required to compensate the phase lag introduced by resonant poles and RHP zero. In this paper, type III compensators are designed to ensure unconditional closed-loop stability as phase-lag approaches 180° at cross-over frequency. The TF of the compensator is,

$$C_{v_i}(s) = \frac{k_{c_i} (s + \omega_{z_i})^2}{s (s + \omega_{p_i})^2}. \quad (2)$$

From (1), it is clear that the RHP zero depends on the steady-state duty cycle, D_i , and the resistive load, R_L . Therefore, the bandwidth is set a decade smaller than the RHP zero frequency to accommodate varying operating conditions e.g. the worst case scenario occurring at maximum duty cycle and minimum load [17].

IV. DISTRIBUTED HIERARCHICAL CONTROL

The dc ImG implemented here consists of boost converters connected to a common dc bus through cables represented by line resistances. The dc bus voltage has been optimally chosen as 380 V by the EMerge Alliance Data/Telecom Centre Standard for LVDC networks. Various loads are subsequently connected to the common dc bus. Fig. 3 below shows the distributed hierarchical droop controlled dc ImG configuration.

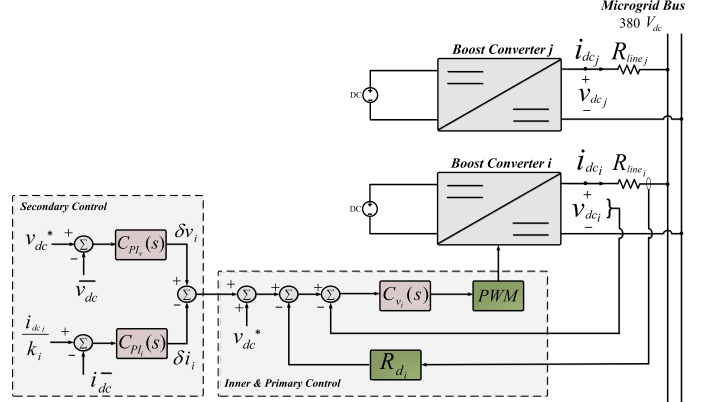


Fig. 3. Distributed hierarchical droop control scheme. Adapted from [14].

In general, it is more difficult to stabilise a large complex network with decentralised or distributed controllers when compared to a centralised controller since system states are only locally or partially known *a priori*. Hence, global asymptotic stability cannot be guaranteed. However, decentralised control of some large-scale systems, such as power networks, is based on the concept of neutral couplings among subsystems [18]. Before designing secondary controllers, it is beneficial to investigate the interaction between the DGUs at the primary level. This will determine whether or not the local type III compensator can be tuned in a decoupled fashion.

A. Primary Droop Control

Droop control is a decentralised, proportional control method, used throughout power networks for load-sharing

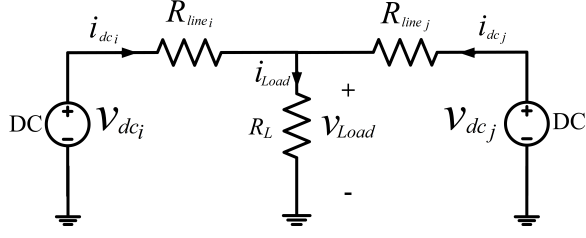


Fig. 4. Equivalent two node network

among multiple sources. Fig. 3 is electrically equivalent to the simple two-node network shown below.

Performing nodal analysis yields:

$$v_{dc_i} = i_{dc_i} R_{line_i} - i_{load} R_L, \quad (3)$$

$$i_{dc_i} = \alpha_i v_{dc_i} - \beta v_{dc_j}, \quad (4)$$

$$\text{where } \alpha_i = \frac{R_{line_j} R_L}{R_{line_i} R_{line_j} + R_{line_i} R_L + R_{line_j} R_L} \text{ and } \beta = \frac{R_L}{R_{line_i} R_{line_j} + R_{line_i} R_L + R_{line_j} R_L}.$$

From (4), power delivered to the load is dependent on the voltage difference between each DGU. However, voltage differences induce circulation currents; potentially overloading each DGU. To minimise circulation currents and control the current-sharing ability of each DGU, a virtual resistance is introduced to adjust the local voltage reference. The proportional control action, enables current-sharing by linearly decreasing the DGU output voltage as load demand increases.

As outlined in [14], droop control has two limitations - voltage deviation and inaccurate current-sharing. Voltage deviation inherently exists between the reference and DGU output voltage due to the proportional control action. From Fig. 3, droop control can be expressed as,

$$v_{dc_i} = v_{dc}^* - i_{dc_i} R_{d_i} \quad ; \quad \Delta v_{dc} = i_{dc_i} R_{d_i}. \quad (5)$$

From (5), a deviation from the reference always exists, except during no-load. Furthermore, the existence of varying voltage drops across different line resistances between the DGUs and the common dc bus creates further voltage deviations throughout the system; this results in poor voltage restoration.

Second, the presence of line resistances, along with virtual resistances, degrades current-sharing accuracy. The current-sharing ratio is derived as:

$$\frac{i_{dc_i}}{i_{dc_j}} = \frac{R_{d_j}}{R_{d_i}} + \frac{R_{line_j} - R_{line_i} \frac{R_{d_j}}{R_{d_i}}}{R_{d_i} + R_{line_j}}. \quad (6)$$

Ideally, the current-sharing ratio is exclusively dependent on the virtual resistances. This is realisable when $R_{d_i} \gg R_{line_i}$. However, R_{d_i} is limited by the ratio between DGU voltage deviation and no-load current, while large droop coefficients challenge stability [14]. Distributed secondary control loops are employed to overcome these limitations of primary control.

B. Consensus-Based Secondary Control

Secondary control is employed to manage mG power quality outside the primary droop control layer at a slower bandwidth; types of secondary controllers are reviewed in [14], [16]. Large communication and computation complexity should be

minimised in a mG consisting of distributed elements. As a result, distributed techniques using low-bandwidth communications have been developed. Distributed coordination among DGUs can be achieved using consensus algorithms. Consensus algorithms help DGUs gain global awareness with limited information. A simple consensus protocol involving average measurements of adjacent DGU currents and voltages is used to modulate the set-points of each local controller as seen in Fig. 3. By implementing the PI controller (7) to drive the average voltage \bar{v}_{dc} of neighbouring DGUs to v_{dc}^* , voltages in the grid can be maintained within a desired range.

$$\delta v_i = k_{p\bar{v}_i} (v_{dc}^* - \bar{v}_{dc}) + k_{i\bar{v}_i} \int (v_{dc}^* - \bar{v}_{dc}) dt. \quad (7)$$

Similarly, to improve the current-sharing accuracy, a PI controller is implemented to drive the average output current \bar{i}_{dc_i} to a proportion of each DGU output current, defined by parameters k_i, k_j . Equal-current-sharing is achieved by setting $k_i = k_j$.

$$\delta i_i = k_{p\bar{i}_i} \left(\frac{i_{dc_i}}{k_i} - \bar{i}_{dc} \right) + k_{i\bar{i}_i} \int \left(\frac{i_{dc_i}}{k_i} - \bar{i}_{dc} \right) dt. \quad (8)$$

However, the use of classical SISO controllers in a MIMO system limits the tuning of each average voltage and current PI controller to an iterative trial and error task [19], [20].

V. DYNAMICS OF INTERACTING CONVERTERS

In order to design local decentralised controllers, a global model of the system is initially required. Subsequent interaction analysis can determine if couplings are neutral; the system can then be decomposed into local elements [18]. Interactions between DGUs are expressed through duty cycle cross-coupling and coupling via line resistances. The duty cycle cross-coupling between the two open-loop converters can be represented as:

$$\begin{bmatrix} \tilde{v}_{dc_i}(s) \\ \tilde{v}_{dc_j}(s) \end{bmatrix} = \begin{bmatrix} G_{ii}(s) & G_{ij}(s) \\ G_{ji}(s) & G_{jj}(s) \end{bmatrix} \begin{bmatrix} \tilde{d}_i(s) \\ \tilde{d}_j(s) \end{bmatrix}. \quad (9)$$

The global open-loop TF representing i - i pairings, which accounts for line resistance coupling and dynamics of both DGUs, is:

$$G_{ii}(s) = \frac{-V_{in_i}}{(1 - D_i)} \frac{a_0 s^3 + a_1 s^2 + a_2 s + a_3}{b_0 s^4 + b_1 s^3 + b_2 s^2 + b_3 s + b_4}; \quad (10)$$

$$a_0 = C_i L_i L_j; a_1 = L_j (L_i \alpha_j - C_j \alpha_i); a_2 = (L_i D_i^2 + L_i - 2L_i D_i - L_i \alpha_i \alpha_j); a_3 = \alpha_i (1 - D_j)^2; b_0 = C_i C_j L_i L_j + L_i L_j; b_1 = C_j \alpha_i + C_i \alpha_j; b_2 = C_i L_i + C_j L_j - 2C_i D_j L_i + L_i L_j \alpha_j - 2C_j D_i L_j + C_i D_j^2 L_i + C_j D_i^2 L_j - L_i L_j \beta^2; b_3 = L_i \alpha_i + L_j \alpha_j + D_j^2 L_i \alpha_i + D_i^2 L_j \alpha_j - 2D_j L_i \alpha_j; b_4 = D_i^2 - 2D_j - 2D_i D_j^2 - 2D_i^2 D_j - 2D_i + D_j^2 + D_i^2 D_j^2 + 4D_i D_j + 1.$$

The cross-coupling open-loop TF, representing how v_{dc_i} is influenced by d_j , is:

$$G_{ij}(s) = \frac{-V_{in_j}}{(1 - D_j)} \frac{L_i \beta s (L_j s - \alpha_j)}{b_0 s^4 + b_1 s^3 + b_2 s^2 + b_3 s + b_4}, \quad (11)$$

where $G_{ji}(s)$ and $G_{jj}(s)$ are of the same form as (11) and (10) respectively, with subscripts interchanged.

A good measure of dynamic interaction between subsystems is the steady-state RGA [19]. Each element of the RGA in

(12) defines interactions as a ratio between the open-loop and closed-loop gains of i - i , i - j pairings etc., or effectively, the ratio between an uncoupled DGU and coupled DGU [19], as represented by (13). The closed-loop gain accounts for the effect that \tilde{d}_j has on \tilde{v}_{dc_i} in response to a change in \tilde{d}_i .

$$\Lambda = \begin{bmatrix} \lambda_{ii} & \lambda_{ij} \\ \lambda_{ji} & \lambda_{jj} \end{bmatrix} = \begin{bmatrix} \lambda_{ii} & 1 - \lambda_{ii} \\ 1 - \lambda_{jj} & \lambda_{jj} \end{bmatrix}, \quad (12)$$

$$\lambda_{ii} = \frac{G_{ii}(s)(1 + C_{v_j}(s)G_{jj}(s))}{G_{ii}(s) + C_{v_j}(s)(G_{ii}(s)G_{jj}(s) - G_{ij}(s)G_{ji}(s))}. \quad (13)$$

In general, pairings are preferred if the diagonal elements of $\Lambda \approx 1$ at the cross-over frequency, as interactions from another loop do not cause instability. A negative steady-state value of Λ means that the gain has changed when the system is affected by the control input of another loop, resulting in undesirable interactions; such pairings are to be avoided [20].

TABLE I
STEADY-STATE RGA AT DIFFERENT FREQUENCIES

Frequency (rads ⁻¹)	RGA
10	$\begin{bmatrix} 1.0001 & -0.0001 \\ -0.0001 & 1.0001 \end{bmatrix}$
100	$\begin{bmatrix} 1.0032 & -0.0068 \\ -0.0068 & 1.0032 \end{bmatrix}$
1000	$\begin{bmatrix} 1.4354 & -0.4354 \\ -0.4354 & 1.4354 \end{bmatrix}$
2220	$\begin{bmatrix} 1.0245 & -0.0245 \\ -0.0245 & 1.0245 \end{bmatrix}$
5000	$\begin{bmatrix} 1.0030 & -0.0030 \\ -0.0030 & 1.0030 \end{bmatrix}$

From Table I, steady-state interactions between coupled DGUs are neutral, appearing to allow the design of decentralised controllers. These results are based on system parameters in Table II of section VI. Interactions are most significant approaching the cross-over frequency. This results in resonant-pole damping (i.e. due to the added effect of \tilde{d}_j on \tilde{v}_{dc_i}). This can be seen by comparing the decoupled DGU i in (1) and coupled DGU i , as represented by the TF;

$$\frac{\tilde{v}_{dc_i}(s)}{\tilde{d}_i(s)} = G_{ii}(s) - \frac{C_{v_j}(s)G_{ij}(s)G_{ji}(s)}{1 + C_{v_j}(s)G_{jj}(s)}. \quad (14)$$

The effect of the coupled DGUs changes the RHP zero of each DGU from being load dependant $\omega_{rhp_i} = \frac{(1-D_i)R_L}{L_i}$ to being line dependent $\omega_{rhp_i} = \frac{\alpha_i}{L_i}$. Since small impedances in parallel networks dominate, the RHP zero frequency reduces by 16971 rads⁻¹, further limiting the bandwidth and performance. Consequently, controller detuning is required, as seen in section VI.

Ultimately, with neutral interactions a decentralised controller can be designed, as in the case of buck converters. However, when controlling boost converters in a dc ImG, global knowledge of coupling is required to account for variation in the RHP zero in order for appropriate controller tuning. It is also worth noting that in small-scale networks, where line resistances are small, the RHP zero frequency is lower than in larger networks, requiring a slower bandwidth.

VI. SIMULATION TESTS

Controllers and simulations were developed in Matlab/Simulink software. For greater accuracy this work uses non-linear PWM driven boost converter designed in the simpowersystems toolbox, according to [17], as opposed to [13]–[15] which use averaged buck converter models. Design parameters and controller gains are presented in Table II for DGU i . As this paper deals with a homogeneous system, DGU $i = \text{DGU } j$.

TABLE II
ELECTRICAL AND CONTROL PARAMETERS

Description	Parameter	Value
DGU rated power	P	5 kW
Input voltage	V_{in_i}	50 V
Reference voltage	v_{dc}^*	380 V
Switching frequency	f_s	25 kHz
Duty cycle	D_i	0.8684
Inductance	L_i	90.21 μ H
Capacitance	C_i	363.16 μ F
DGU i line resistance	R_{line_i}	4 Ω
DGU j line resistance	R_{line_j}	1 Ω
Droop co-efficient	R_{d_i}	2.66 Ω
Compensator gain	k_{c_i}	354.71
Compensator zero frequency	ω_{z_i}	201.72 rads ⁻¹
Compensator pole frequency	ω_{p_i}	18260 rads ⁻¹
Average voltage proportional gain	$k_{p\bar{v}_i}$	1.81
Average voltage integral gain	$k_{i\bar{v}_i}$	8
Average current proportional gain	$k_{p\bar{i}_i}$	17.4
Average current integral gain	$k_{i\bar{i}_i}$	81

A. Ideal voltage restoration & current-sharing with load steps

Primary controllers were initially tuned in a decoupled fashion to highlight the limited performance. Ideal DGU voltage and current-sharing responses under load power disturbances, P_{RL} , are obtained. These responses are ideal in the sense that communication between DGUs is assumed to be perfect i.e. infinite bandwidth. P_{RL} is nominally set to 1 kW.

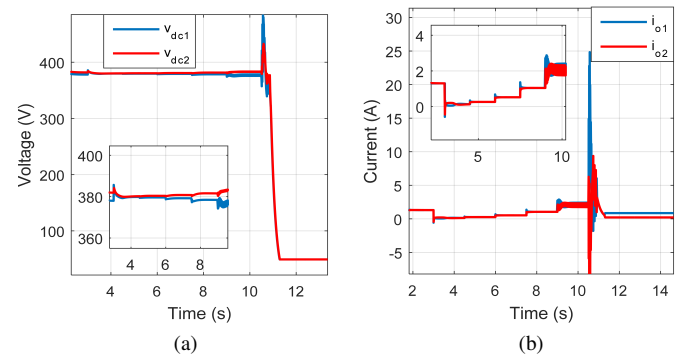


Fig. 5. Ideal voltage restoration and current-sharing with load disturbances

P_{RL} is stepped from 0.1 - 3.2 kW, doubling every 1.5 s. Fig. 5(a) shows that ideal voltage restoration, where the average voltage over the DGUs is regulated to v_{dc}^* , is achieved until 10.5 s. At this point the system becomes unstable when P_{RL} is 3.2 kW. The duty cycle of each DGU saturates, effectively opening each control loop. Ideal equal-current-sharing is shown in Fig. 5(b) to have a considerably faster settling time than [14] of 200 ms, up until when P_{RL} is 3.2 kW, after which equal-current-sharing is lost.

Ultimately, decoupled tuning of the inner controllers achieves an operating range of up to an instability onset of 2 kW. As discussed, each compensator requires detuning in order to extend the range of stability and performance.

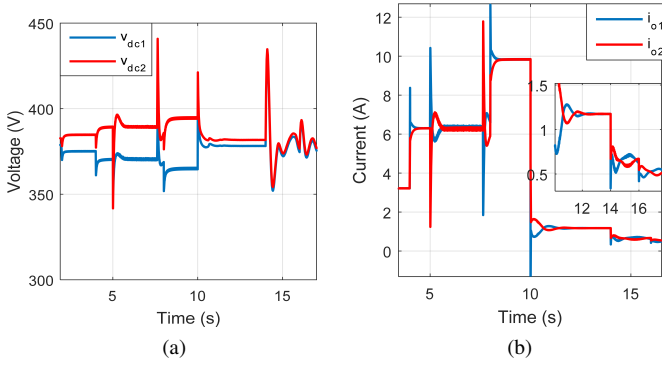


Fig. 6. Detuned ideal voltage restoration and current-sharing with disturbances

Inner controllers were detuned to accommodate a reduced RHP zero frequency, $\omega_{rhp_i} = 2287 \text{ rad/s}$. Fig. 6 shows ideal responses to step changes of 0.5 - 8 kW in P_{RL} . At 14 s, P_{RL} decreases to 400 W. As the load resistance increases, circulation currents increase along the path of least resistance. Under lighter loads, the converter is forced into discontinuous conduction mode. With this, the model changes, and the voltage responses of each DGU become oscillatory. Buck converters are commonly used to interface low-power loads with 380 V buses, and to create other low voltage buses.

B. Impact of low-bandwidth communication faults

The impact of low-bandwidth communication delays has previously been shown in dc [14] and ac ImGs [21] to destabilise the voltage and frequency restoration respectively, highlighting a trade-off between controller bandwidth and delays. In [14], each communications channel is modelled as a first-order lag. In this paper, using a zero-order-hold model more accurately represents the effect of delay.

A communication fault is introduced after 5 s on DGU i 's measurement of i_{dc_j} . Such a fault can represent packet losses within the communications network of the ImG.

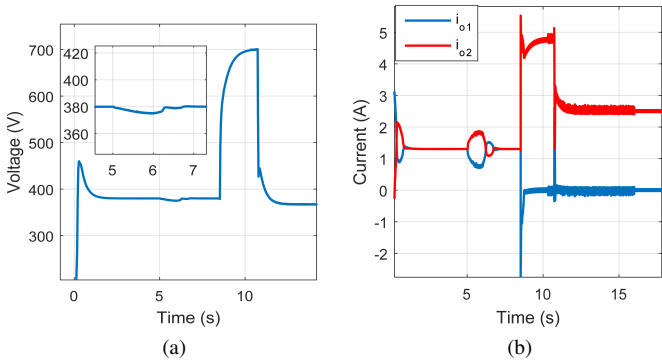


Fig. 7. Voltage restoration & equal-current-sharing with DGU LBC fault

A small voltage sag is observed in Fig. 7(a) for the duration of the fault as the loss of the measurement of i_{dc_j} degrades the ability of the average current PI controller to modulate v_{dc}^* in order to maintain \bar{v}_{dc} at 380 V. Fig. 7(b) shows the loss of equal-current-sharing; though stability is maintained.

After 1 s, communication is regained, and voltage restoration and equal-current-sharing are both restored. At 8 s, a fault is introduced for 2 s on DGU j 's measurement of v_{dc_i} . Fig. 7(a) shows a large voltage increase as only local information is available, driving the voltage reference above rated. Once communication is resumed, voltage restoration is restored with \bar{v}_{dc} regulated to 380 V. However, Fig. 7(b) shows that equal-current-sharing is lost even when communication is restored. DGU j fails to act as a current source for the ImG.

Ultimately, it is difficult to quantify communication delays and faults *a priori*. Therefore, secondary controllers should be conservatively tuned if the system is without an adaptive mechanism.

C. Introduction of PWM speed controlled dc motor load

Large non-linear motor loads are common in C&I buildings. As an example, a 3.8 kW, 500 V, 1775 RPM wound rotor dc motor is connected to the common dc bus. A 300 V dc supply is used to create the electromagnetic field.

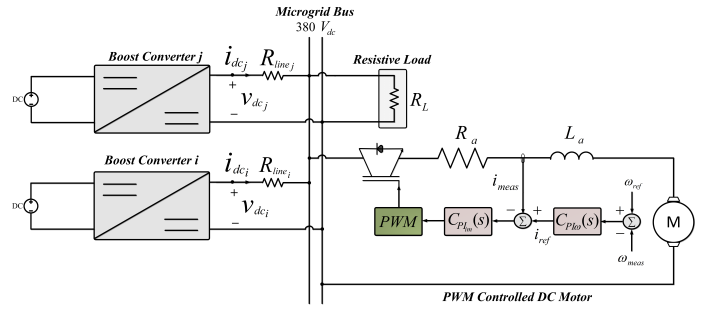


Fig. 8. Closed-loop PWM speed controlled dc motor model

The motor model and cascaded PI controllers were designed according to [22]. The cascade control loops are decoupled by setting the current/torque loop to a bandwidth of 700 Hz and speed loop to a bandwidth of 70 Hz.

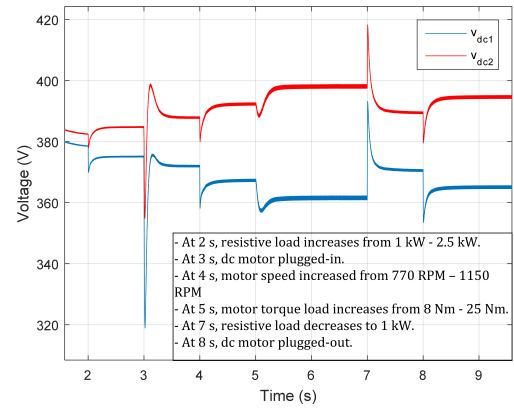


Fig. 9. Voltage restoration with dc motor, P_{RL} & 20 ms LBC delay

Fig. 9 shows that with detuned controllers, the plugging-in, speed and mechanical load change of the dc motor does not adversely affect the performance of the boost converters.

D. Plug-and-Play Capabilities

PnP is the capability of a system to maintain operation stability when devices are reconfigured without *a priori* knowledge. PnP operations enable DGU reconfiguration for features such as redundancy, resiliency, fault-tolerance and cooperation.

This section investigates if the control scheme can maintain system stability upon reconfiguring DGUs and loads within the dc ImG. Two additional boost converters are introduced to the ImG; one cooperates with the original DGUs by employing the hierarchical scheme, while one does not cooperate, employing only inner voltage control. Initially, each DGU is tuned without accounting for coupling. DGUs 1 and 2 are connected while DGU 3 and 4 supply power to local loads. At 3 s, DGU 3 is connected to DGU 1 and 2, and at 4 s, the uncooperative DGU 4 is connected. At 5 s, the dc motor is plugged-in. At 6 s, P_{RL} , which is predominantly powered by DGUs 1, 2 and 3, increases from 2 - 8 kW. As seen in Fig. 10(a), voltages become oscillatory. At this point each DGU duty cycle is saturated, collapsing the ImG's voltage levels.

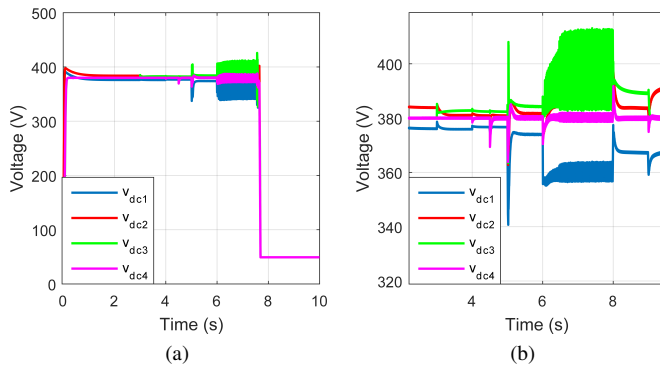


Fig. 10. PnP instability with decoupled tuning & PnP enabled with detuning.

To highlight the lack of PnP capabilities with conventionally tuned controllers, DGU 1 and 2 are detuned, accounting for coupling as before. Fig. 10(b) shows that voltage restoration is maintained when P_{RL} increases to 8 kW at 6 s, and when the dc motor and DGU 3 are plugged-out at 8 and 9 s respectively. Reconfigurability can be achieved if controllers have a mechanism for changing their parameters on-line; further justifying the future use of adaptive control in mGs.

VII. CONCLUSION

This work extends the state-of-the-art dc ImG distributed hierarchical control architecture to dc-dc boost converters. The use of classical controllers at primary and secondary levels is shown to achieve voltage restoration and accurate current-sharing when typical linear and non-linear loads are connected. Communication faults highlight the need for estimation, or event-based communications in order to improve fault-tolerance. The paper demonstrates the technique's lack of scalability. Though RGA analysis indicates that the design of local controllers does not require knowledge of neighbouring DGUs and their controllers, global knowledge of line couplings is required. The PnP capability of this scheme is limited; on-line modification of control parameters is required to maintain stability as DGUs and loads are added/removed. The state-of-the-art PnP techniques recently applied in dc [13] and ac [23] ImGs have achieved success in guaranteeing scalable PnP voltage stability in both radial and meshed mGs. However, this technique demonstrates poor robustness to uncertainty.

Ultimately, the control design presented in this paper is monolithic. Scalable and robust-adaptive controls are needed

to further improve the autonomy of mGs that are defined by heterogeneity, uncertainty and changing conditions.

ACKNOWLEDGEMENT

This work was funded by the IRC enterprise partnership scheme in collaboration with UCC and UTRC-Ireland Ltd.

REFERENCES

- [1] R. Lasseter, "MicroGrids," *IEEE Power Engineering Society Winter Meeting*, vol. 1, p. IEEE, 2002.
- [2] J. M. Guerrero, M. Chandorkar, T. L. Lee, and P. C. Loh, "Advanced control architectures for intelligent microgrids: Part I: Decentralized and hierarchical control," *IEEE Trans. Ind. Electron.*, vol. 60.4, pp. 1254–1262, 2013.
- [3] J. M. Guerrero, P. C. Loh, T. L. Lee, and M. Chandorkar, "Advanced control architectures for intelligent microgrids: Part II: Power quality, energy storage, and AC/DC microgrids," *IEEE Trans. Ind. Electron.*, vol. 60.4, pp. 1263–1270, 2013.
- [4] D. P. Symanski, "Residential & Commercial Use Of DC Power," 2011.
- [5] B. T. Patterson, "DC, Come Home: DC Microgrids and the Birth of the 'Enernet'," *IEEE Power and Energy Magazine*, vol. 10, no. 6, pp. 60–69, 2012.
- [6] D. J. Becker and B. J. Sonnenberg, "DC microgrids in buildings and data centers," in *Telecom. Energy Conference (INTELEC)*, 2011.
- [7] A. T. Elsayed, A. A. Mohamed, and O. A. Mohammed, "DC microgrids and distribution systems: An overview," *Electric Power Systems Research*, vol. 119, pp. 407–417, 2015.
- [8] E. R. Diaz, X. Su, M. Savaghebi, J. C. Vasquez, M. Han, and J. M. Guerrero, "Intelligent DC microgrid living laboratories - A Chinese-danish cooperation project," *IEEE 1st ICDCM*, pp. 365–370, 2015.
- [9] Z. Jin, M. Savaghebi, J. C. Vasquez, L. Meng, and J. M. Guerrero, "Maritime DC microgrids - A combination of microgrid technologies and maritime onboard power system for future ships," *IEEE 8th IPEMC-ECCE Asia*, pp. 179–184, 2016.
- [10] D. Van Hertem and M. Ghandhari, "Multi-terminal VSC HVDC for the European supergrid: Obstacles," *Renewable and Sustainable Energy Reviews*, vol. 14, no. 9, pp. 3156–3163, 2010.
- [11] T. Dragicevic, X. Lu, J. C. Vasquez, and J. M. Guerrero, "DC Microgrids - Part I: A Review of Control Strategies and Stabilization Techniques," *IEEE Trans. on Power Electron.*, vol. 31.7, pp. 4876–4891, 2016.
- [12] J. M. Guerrero, J. C. Vasquez, J. Matas, L. G. De Vicuña, and M. Castilla, "Hierarchical control of droop-controlled AC and DC microgrids - A general approach toward standardization," *IEEE Trans. Ind. Electron.*, vol. 58.1, pp. 158–172, 2011.
- [13] M. Tucci, S. Rivero, J. C. Vasquez, J. M. Guerrero, and G. Ferrari-Trecate, "Voltage control of DC islanded microgrids : a decentralized scalable approach," in *IEEE 54th Annual Conf. on Decision and Control*, 2015, pp. 3149–3154.
- [14] X. Lu, J. M. Guerrero, K. Sun, and J. C. Vasquez, "An improved droop control method for dc microgrids based on low bandwidth communication with dc bus voltage restoration and enhanced current sharing accuracy," *IEEE Trans. on Power Electron.*, vol. 29.4, pp. 1800–1812, 2014.
- [15] Q. Shafiee and E. Al, "Modeling, stability analysis and active stabilization of multiple DC-microgrid clusters," in *IEEE ENERGYCON*, 2014, pp. 1284–1290.
- [16] P. Wang, X. Lu, X. Yang, W. Wang, and D. Xu, "An Improved Distributed Secondary Control Method for DC Microgrids with Enhanced Dynamic Current Sharing Performance," *IEEE Trans. on Power Electron.*, vol. 31.9, pp. 6658–6673, 2016.
- [17] N. Mohan, *Power Electronics - A First Course*. MNPERE, 2009.
- [18] J. Lunze, *Feedback Control of Large-Scale Systems*. London: Prentice-Hall, 1992.
- [19] J. Pierre-Corriu, *Process Control Theory and Applications*, 2013.
- [20] S. Skogestad and I. Postlethwaite, "Multivariable feedback control: analysis and design," Wiley, vol. 2, 2007.
- [21] S. Liu, X. Wang, and P. X. Liu, "Impact of Communication Delays on Secondary Frequency Control in an Islanded Microgrid," *IEEE Trans. Ind. Electron.*, vol. 62.4 2015, pp. 2021–2031.
- [22] N. Mohan, *Advanced Electric Drives: analysis, control, and modeling using MATLAB/Simulink*, 2014, vol. 53, no. 9.
- [23] S. Rivero, F. Sarzo, and G. Ferrari-Trecate, "Plug-and-Play Voltage and Frequency Control of Islanded Microgrids with Meshed Topology," *IEEE Transactions on Smart Grid*, vol. 6, no. 3, pp. 1176–1184, 2015.